Nanoscale

Cite this: *Nanoscale*, 2011, **3**, 4962

www.rsc.org/nanoscale

COMMUNICATION

Single-crystal like mesoporous ZnO:Mn^{2+} nanorings of high optoelectronic quality formed by self-assembly of nanoparticles in an ultrasonic hydrolysis process†

Umapada Pal,[a] Chang Woo Kim,[b] Kyujoon Lee,[c] Myung-Hwa Jung[c] and Young Soo Kang*[b]

Received 3rd August 2011, Accepted 1st October 2011
DOI: 10.1039/c1nr11007a

Unique ring-shaped single-crystal like mesoporous ZnO:Mn^{2+} nanostructures have been fabricated through ultrasound assisted hydrolysis of zinc and manganese precursors. Incorporation of manganese into the nanostructures induced soft ferromagnetic behaviour. The nanostructures are of high optoelectronic quality with little structural and electronic defects. A mechanism of formation of the novel porous structures is proposed. The presence of manganese in Mn^{2+} state with strong hyperfine splitting (89 G) promises the application of these porous nanostructures in designing nanometric spintronic devices.

Self-assembled nanostructures are the building blocks for fabricating nano-devices through bottom-up processes. While fabrication of such self-assembled nanostructures is a challenging task, understanding their formation process is essential for improving their performance and functionality in devices. Formation of several self-assembled metal oxide nanostructures like polyhedral cages,[1] tetrahedral superlattices,[2] spirals, gyroids, flower-like,[3] and several hierarchically ordered mesophase crystals[4–9] has been reported. On the other hand, several modifications on those nanostructures have been realized to induce new functionalities in them.

In the present article, we report on the fabrication of single-crystal like mesoporous ring-shaped ZnO:Mn^{2+} nanostructures formed by the self-assembly of very small nanoparticles during the ultrasound assisted hydrolysis process. Incorporation of Mn ions into these unique shaped nanostructures induced soft ferromagnetic behavior. Structure, porosity, magnetic, and optoelectronic properties of the nanostructures are studied. A mechanism for the growth of such novel structures is proposed.

[a]*Instituto de Física, Universidad Autónoma de Puebla, Apdo. Postal J-48, Puebla, Pue., 72570, Mexico*
[b]*Department of Chemistry, Sogang University, Seoul, 121-742, Republic of Korea. E-mail: yskang@sogang.ac.kr; Fax: +82 2 701 0967; Tel: +82 2 705 8882*
[c]*Department of Physics, Sogang University, Seoul, 121-742, Republic of Korea*

† Electronic supplementary information (ESI) available: Details of the experimental procedure, including some typical TEM and HRTEM images of the mesoporous Mn^{2+}:ZnO structures. See DOI: 10.1039/c1nr11007a

Zinc oxide is a high band gap material (3.37 eV at 300 K) with versatile characteristics and applications such as in catalysis,[10,11] sensors,[12] and optoelectronic devices.[13,14] In porous form, it should have even higher catalytic activities due to high specific surface area. Recently mesoporous zinc oxide has been fabricated through ultrasound assisted hydrolysis of zinc acetate,[15–17] liquid crystal templating or exotemplating with mesoporous carbon.[18] On the other hand, fabrication of micrometre size ZnO disk and ring structures in large scale has been reported by Li *et al.*[19]

We prepared mesoporous ZnO:Mn^{2+} nanostructures of high optoelectronic qualities through ultrasound assisted hydrolysis of zinc (II) acetate dihydrate by modifying the process reported in our previous work.[15] In a typical synthesis process, 1.5 g of zinc(II) acetate dihydrate and 135 mg (10 mol%) of manganese chloride were mixed in 100 ml *N*,*N*-dimethylformamide and deionized water mixture (9 : 1, v/v) under magnetic stirring. The mixture solution was then ultrasonicated for 3 h at 250 W power, using an ultrasonic T-horn under Ar bubbling. Usefulness of water and argon bubbling during the ultrasonic hydrolysis process of zinc acetate has been reported earlier.[15,16] The obtained white precipitate was washed with ethanol several times, separated by centrifugation, and dried at 60 °C in air.

As can be seen from Fig. 1, the undoped ZnO nanostructures are mostly of hexagonal shape with about 200 nm average diameter, formed through self-assembly of small (~3 nm) nanoparticles. Presence of a good fraction of triangular shaped particles confirms that the hexagonal structures are formed through the self-assembly of triangular structures (Fig. 1a). Formation of unique hexagonal ring structures was observed only for ZnO:Mn^{2+} samples (Fig. 1b). As can be perceived from Fig. 1b, more than 40% of the nanostructures form complete hexagonal rings. The nitrogen adsorption–desorption isotherm of the nanostructures (Fig. 2d) revealed mesoporous nature of their walls, with type II adsorption behaviour. The estimated BJH average pore diameter and specific surface area of the ZnO:Mn^{2+} sample were 2.17 nm and 47.3 $m^2\ g^{-1}$, respectively. The specific surface area of these ring shaped mesoporous nanostructures is substantially higher than the reported values for ZnO mesostructures.[15,16,20]

Excellent crystalline nature of the nanostructures can be observed from the intense, narrow X-ray diffraction peaks (Fig. 2a) and well ordered lattice planes in their high resolution TEM images (Fig. 1c, also see Fig. S2†), even at their curved edges. Though the presence of

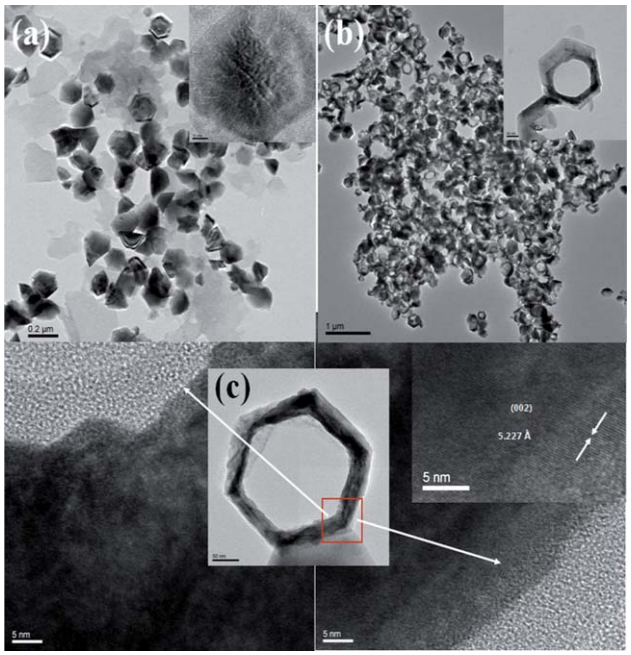

Fig. 1 Typical TEM images of (a) undoped ZnO nanostructure, (b) ZnO:Mn^{2+} nanostructure, and (c) HRTEM of the inner and outer parts of the corner of a nanoring structure. Highly ordered crystalline nature of the nanoring structure is shown in the inset of (c).

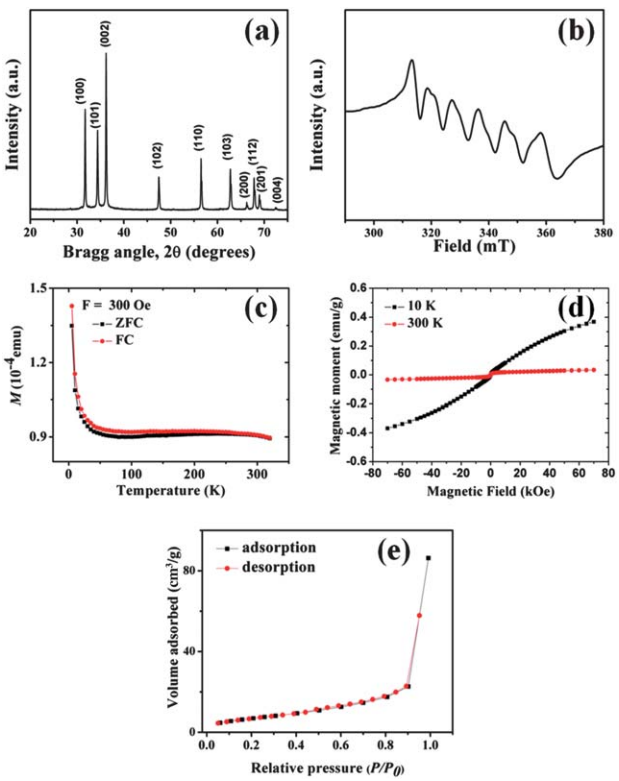

Fig. 2 (a) XRD pattern, (b) ESR spectrum (c) FC/ZFC magnetization curves, (d) magnetization hysteresis, and (e) N_2 absorption–desorption isotherm of the ZnO : Mn^{2+} nanoring structures.

Mn in ring structures was difficult to monitor through EDS elemental mapping (Fig. 3, top row), XPS analysis (Fig. 4) and the room temperature ESR spectrum revealed clearly the presence of manganese in Mn^{2+} state (Fig. 2b). In spite of 10 mol% nominal doping, XPS analysis revealed considerably lower manganese (~0.8 atom%) content in the nanostructures. The X-band ESR spectrum revealed a sextet splitting broad signal, characteristic of the hyperfine coupling of Mn^{2+} ($I = 5/2$), with an apparent hyperfine splitting constant of *ca.* 89 G and a g factor of 2.03574. This is consistent with the previous reports[21,22] and indicates that Mn^{2+} ions are homogeneously dispersed into the ZnO frameworks as revealed in EDS elemental mapping (Fig. 3, top row). Soft ferromagnetic behaviour of the ring structures is clear from the difference in their temperature dependent magnetization curves (Fig. 2c) recorded for field cooling (FC) and zero field cooling (ZFC). Both the ZFC and FC decreased with temperature up

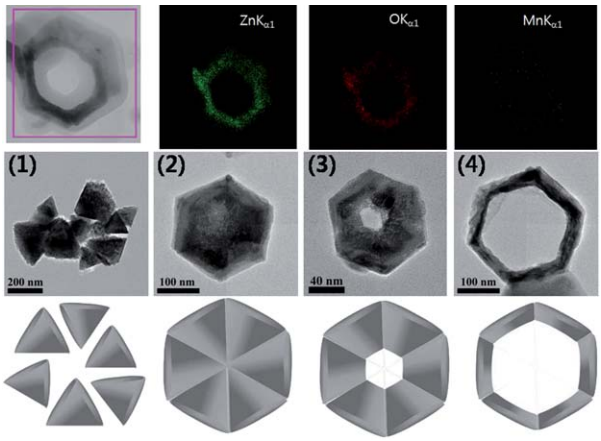

Fig. 3 EDS elemental mapping of different elements on a ZnO:Mn^{2+} nanoring (top row); morphology evolution at different stages of formation (middle row), and schematic presentation of sequential formation steps (bottom row) of the nanoring structures.

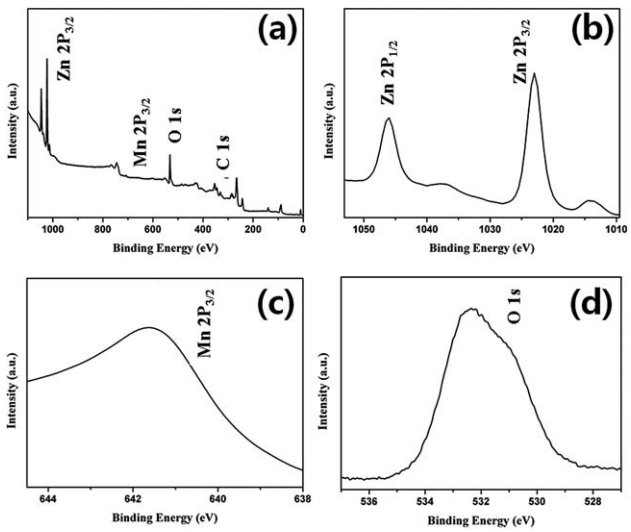

Fig. 4 XPS (a) survey, and high resolution spectra at the (b) Zn, (c) Mn and (d) O emission regions for the ZnO:Mn^{2+} nanostructures. The two components of the O 1s band correspond to the interaction of O with zinc and manganese (see Fig. S4 of the ESI†).

to ~80 K, and then increased marginally. Below 200 K, the magnetization values of ZFC and FC differ significantly indicating their spin-glass behaviour at low temperature.[23] The 300 K hysteresis loop of the as-grown ZnO:Mn^{2+} sample (Fig. 2d) revealed its soft magnetic character like a dilute magnetic semiconductor (DMS). The saturation magnetization increased up to 0.37 emu g^{-1} at 10 K. However, the coercivity of the sample was low (~13 Oe).

Formation of the nanoring structures can be understood through the schematically presented steps at the bottom row of Fig. 3. As stated earlier, the hexagonal sheet structures (~200 nm diameter) are formed through the self-assembly of porous triangles of similar dimensions exposing their high energy polar surfaces (positively charged Zn (0001) and negatively charged O ($000\bar{1}$) planes) vertically. On formation of such hexagonal structures of lowest surface energy, their central parts remain most defective due to stacking defects (stacking faults). On prolonged sonication at high power, the defective central part of the nanostructures starts dissolving due to sonication induced heating. While the acidic nature of the reaction solution helps to dissolve zinc oxide at such high temperature, lower thermal conductivity of MnO (~0.25 W mK^{-1}) in comparison with ZnO (0.65–0.95 W mK^{-1}, depending on the impurity content)[24] enhances the dissolution process. Therefore, on high power sonication, the ring shaped nanostructures are formed first by dissolving the central parts and then whole interior of the hexagonal sheets. For even longer sonication time, the ring shaped nanostructures can be broken due to dissolution of their peripheral regions as evidenced from the inset of Fig. 1b.

High optoelectronic quality of the nanostructures can be appreciated from their room temperature photoluminescence (PL) and Raman spectra (Fig. 5). As can be observed, the PL spectrum of the ZnO:Mn^{2+} sample revealed an intense near band edge (NBE) emission at about 372.0 nm (~3.33 eV) with very little emission in the visible region. A small blue-shift of the near band edge emission in comparison with the pure ZnO sample (NBE at 376.5 nm, ~3.29 eV) is due to the incorporation of Mn in the divalent state (NBE of MnO ≈ 3.9 eV). The small hump appeared in the PL spectrum of the ZnO:Mn^{2+} sample spanning between 400 and 450 nm is the contribution of the so-called blue emission in ZnO induced by the neutral oxygen vacancy V_o at the non-depleted surface region.[25] Generally a broad PL emission in the visible region appears for ZnO nanostructures due to structural and compositional disorders. For comparison, the room temperature PL spectrum of a ZnO nanostructure sample of triangle morphology[26] is also presented in Fig. 5a. As can be seen, both the undoped and Mn-doped nanostructures fabricated by the ultrasound assisted hydrolysis process are optoelectronically superior to the similar nanostructures prepared by the thermolysis process. The Raman spectrum of the sample revealed all the fundamental phonon bands of ZnO, along with higher order and multi-phonon ones.[27] However, due to Mn incorporation, two fundamental nonpolar E_2 modes of wurtzite ZnO shifted a little bit (E_2 (low) ≈ 14 cm^{-1} and E_2 (high) ≈ 3 cm^{-1}, respectively) and a few low intensity bands associated with Mn_3O_4 phase[28] appeared. The E_2 (low) and E_2 (high) modes in ZnO correspond to the vibrations of Zn and O sublattice, respectively, and due to incorporation of Mn at Zn lattice site the former is expected to shift much more than the latter.[29] A fractional down-shift of the E_2 (low) mode frequency suggests an overall softening of ZnO lattice upon Mn doping.

In summary, we could fabricate novel ring-shaped, highly crystalline, porous ZnO:Mn^{2+} nanostructures through ultrasound assisted hydrolysis of the zinc and Mn precursors. The ring structures exhibit unique hexagonal geometrical shape, with mesoporous walls composed of self-assembled tiny particles of ~3 nm. While the incorporation of manganese into the nanostructures induces soft magnetic behaviours, presence of manganese in Mn^{2+} state with strong hyperfine splitting (89 G) promises their utilization in nanometric spintronic devices. On the other hand, these porous nanostructures of high specific surface area should be attractive candidates for photocatalytic applications, and the particular shape of the nanostructures opens up the possibility of using them as the magnetic field gradient electrode in fuel cells,[30] batteries, and oxygen concentrators,[31] and anisotropic devices such as magnetic logic in ring-shaped tunnel junction structures.

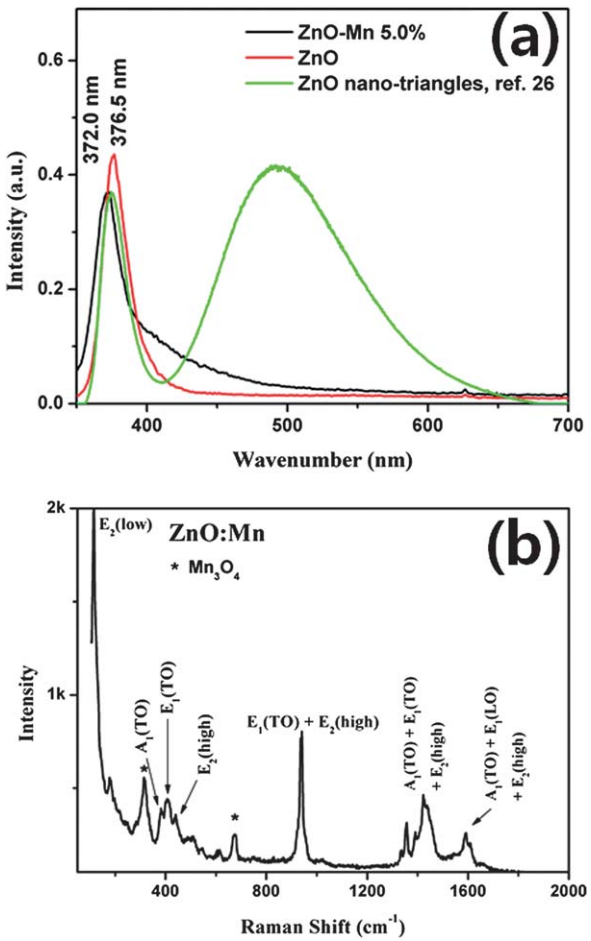

Fig. 5 Room temperature PL (a) and Raman (b) spectra of the ZnO:Mn^{2+} sample. For comparison, a PL spectrum of ZnO sample prepared by the same process, and a PL spectrum of ZnO nanostructure of triangular morphology prepared by thermolysis (ref. 26) have been presented alongside. All the PL spectra were recorded on exciting the samples by a He–Cd laser (λ = 325 nm).

U. Pal thanks Brain Pool Korea for financial support through Brain Pool program. This work was supported by Basic Science Research Program through the National Research Foundation of Korea (NRF) grant funded from the Ministry of Education, Science and Technology (MEST) of Korea for the Center for Next Generation Dye-Sensitized Solar Cells (no. 2010-0001842) and for The Korea Center for Artificial Photosynthesis (NRF-2009-C1AAA001-2009-0093879).

Notes and references

1 P. X. Gao and Z. L. Wang, *J. Am. Chem. Soc.*, 2003, **125**, 11299.
2 J. S. Yin and Z. L. Wang, *Phys. Rev. Lett.*, 1997, **79**, 2570.
3 L.-S. Zhong, J.-S. Hu, H.-P. Liang, A.-M. Cao, W.-G. Song and L.-J. Wan, *Adv. Mater.*, 2006, **18**, 2426.
4 Z. R. R. Tian, J. Liu, J. A. Voigt, B. McKenzie and H. F. Xu, *Angew. Chem., Int. Ed.*, 2003, **42**, 413.
5 H. Shibata, T. Ogura, T. Mukai, T. Ohkubo, H. Sakai and M. Abe, *J. Am. Chem. Soc.*, 2005, **127**, 16396.
6 H. Shibata, H. Mihara, T. Mukai, T. Ogura, H. Kohno, T. Ohkubo, H. Sakai and M. Abe, *Chem. Mater.*, 2006, **18**, 2256.
7 V. N. Urade and H. W. Hillhouse, *J. Phys. Chem. B*, 2005, **109**, 10538.
8 D. Grosso, G. J. de A. A. Soler-lllia, E. L. Crepaldi, F. Cagnol, C. Sinturel, A. Bourgeois, A. Brunet-Bruneau, H. Amenitsch, P. A. Albouy and C. Sanchez, *Chem. Mater.*, 2003, **15**, 4562.
9 J. H. Pan and W. I. Lee, *Chem. Mater.*, 2006, **18**, 847.
10 E. Evgenidou, K. Fytianos and I. Poulios, *Appl. Catal., B*, 2005, **59**, 81.
11 Y. Wang, M. Muhler and C. Wöll, *Phys. Chem. Chem. Phys.*, 2006, **8**, 1521.
12 S. C. Minne, S. R. Manalis and C. F. Quate, *Appl. Phys. Lett.*, 1995, **67**, 3918.
13 Y. W. Zhu, H. Z. Zhang, X. C. Sun, S. Q. Feng, J. Xu, Q. Zhao, B. Xiang, R. M. Wang and D. P. Yu, *Appl. Phys. Lett.*, 2003, **83**, 144.
14 (*a*) T. L. Barr, *J. Phys. Chem.*, 1978, **82**, 1801; (*b*) M. Mullet, V. Khare and C. Ruby, *Surf. Interface Anal.*, 2008, **40**, 323.
15 U. Pal, C. W. Kim, N. A. Jadav and Y. S. Kang, *J. Phys. Chem. C*, 2009, **113**, 14676.
16 S. Bhattacharyya and A. Gedanken, *Microporous Mesoporous Mater.*, 2008, **110**, 553.
17 S. Bhattacharyya and A. Gedanken, *J. Phys. Chem. C*, 2008, **112**, 659.
18 S. Polarz, A. V. Orlov, F. Schuth and A.-H. Lu, *Chem.–Eur. J.*, 2007, **13**, 592.
19 F. Li, Y. Ding, P. Gao, X. Xin and Z. L. Wang, *Angew. Chem.*, 2004, **116**, 5350.
20 J. Zhang, S. Wang, M. Xu, Y. Wang, B. Zhu, S. Zhang, W. Huang and S. Wu, *Cryst. Growth Des.*, 2009, **9**, 3532.
21 K. R. Kittilstved and D. R. Gamelin, *J. Am. Chem. Soc.*, 2005, **127**, 5292.
22 N. S. Norberg, K. R. Kittilstved, J. E. Amonette, R. K. Kukkadapu, D. A. Schwartz and D. R. Gamelin, *J. Am. Chem. Soc.*, 2004, **126**, 9387.
23 J. K. Furdyna, *J. Appl. Phys.*, 1998, **64**, R29.
24 D. R. Lide, *CRC Handbook of Chemistry and Physics*, CRC Press, 85th edn, 2004–2005.
25 Z.-M. Liao, H.-Z. Zhang, Y.-B. Zhou, J. Xu, J.-M. Zhang and D.-P. Yu, *Phys. Lett. A*, 2004, **372**, 4505.
26 G. Muñoz-Hernandez, A. Escobedo Morales and U. Pal, *Cryst. Growth Des.*, 2009, **9**, 299.
27 Y. L. Chen, Z. A. Hu, Y. Q. Chang, H. W. Wang, Z. Y. Zhang, Y. Y. Yang and H. Y. Wu, *J. Phys. Chem. C*, 2011, **111**, 2563.
28 F. Buciuman, F. Patcas, R. Cracium and D. R. T. Zahn, *Phys. Chem. Chem. Phys.*, 1999, **1**, 185.
29 F. Decremps, J. Pellicer-Porres, A. M. Saitta, J. C. Chervin and A. Polian, *Phys. Rev. B: Condens. Matter*, 2002, **65**, 092101.
30 J. Leddy, S. Amarasinghe and L. A. Zook, *US Pat.*, 6479176, 2002.
31 J. Leddy and S. Amarasinghe, *US Pat.*, 6514575, 2003.